ACS APPLIED MATERIALS & INTERFACES

RESEARCH ARTICLE

www.acsami.org

Screen-Printable Silver Pastes with Metallic Nano-Zinc and Nano-Zinc Alloys for Crystalline Silicon Photovoltaic Cells

Alex S. Ionkin,*[,†] Brian M. Fish,[†] Zhigang Rick Li,[†] Mark Lewittes,[†] Paul D. Soper,[†] John G. Pepin,[‡] and Alan F. Carroll[‡]

[†]DuPont Central Research & Development, Experimental Station, Wilmington, Delaware 19880-500, United States

[‡]DuPont Microcircuit Materials (MCM), 14 T. W. Alexander Drive, Research Triangle Park, North Carolina 27709, United States

Supporting Information

ABSTRACT: Silver metallization pastes for crystalline silicon PV cells containing nanosized metallic zinc were found to be superior to commercial pastes containing micrometer-sized metallic zinc and micrometer sized zinc oxide in terms of efficiency and firing window. Efficiency performance decreases as the size of the particles increases: nano-Zn > 3.6 μm Zn > 4.4 μm Zn. Advanced electron microscopy techniques were used to investigate the interfacial microstructure between the front-side contact and the Si emitter of nanosized zinc additive based cells fired at temperatures from below to above optimal. These microstructural observations confirmed the possibility of a tunneling mechanism of current flow (a "nano-Ag colloid assisted tunneling" model) in the absence of Ag crystallites. Contact resistance maps were used to guide sampling, leading to a better understanding of the relationship between microstructure and contact resistance. Low contact resistance and higher cell efficiency, especially at under- and overfiring temperature conditions, are due to more uniform silicon nitride etching obtained through the use of nanosized metallic zinc additives.

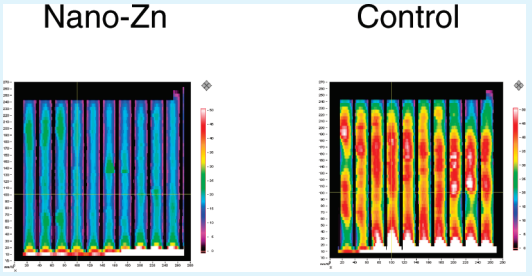

KEYWORDS: photovoltaic, metallization paste, silver, nanozinc, silicon nitride, silicon, microscopy

1. INTRODUCTION

Conductive pastes are important materials in the photovoltaic industry (PV). Silver pastes for crystalline silicon and thin film solar cells are among the most commonly used, and enable solar cells to run more efficiently, last longer and provide environmentally sustainable solutions of alternative energy for everyone. Growth in the PV industry is explosive and there is a continuing need for metallization pastes with increased efficiency and fill factor, as well as a wider processing window.[1−4] The metallization paste must also be able to etch through the protective silicon nitride layer on the front side of the crystalline silicon cells without damaging the emitter layer (Figure 1).[5] Numerous additives for silver metallization pastes were tested and zinc oxide and metallic zinc were found to be the top performers.[6,7]

Silver metallization pastes are heterogeneous systems containing 75−95% by weight of metallic silver powders, and 1−15% by weight of a frit and other inorganic additives. The inorganic components may be mixed with 5−15% by weight of an organic medium to form a viscous "paste" having suitable consistency and rheology for screen-printing. Obviously, particle size and shape play a crucial role in the performance of this paste.[8] It has been reported recently that nanozinc oxide has some advantages over micrometer-sized zinc oxide in PV cells, providing higher efficiencies, denser microstructure and better adhesion.[9−12] The recent availability of large quantities of metallic nanozinc[13] motivated our evaluation of metallic nanozinc and metallic nanozinc alloys as inorganic additives in front-side metallization pastes for crystalline silicon PV devices.

2. EXPERIMENTAL SECTION

Reagents and Materials. Metallic nanozinc is commercially available from Aldrich, Strem and Umicore Inc. (Angleur, Belgium). Dry nanozinc powder exists as agglomerates.[4] The primary particle size of dry nanosized metallic zinc powder is about 100 nm. Upon sonification in an organic solvent, the agglomerates are dissociated to their primary nanoparticles of about 35 nm. The morphology of nanosized metallic zinc is spherical as determined by scanning electron microscopy (SEM) (see Figure 2). The specific surface area of nanosized metallic zinc is between 4 and 6 m^2/g as determined by its BET value. A copper−zinc alloy (56−60 wt % copper and 37−41 wt % zinc) was purchased from Aldrich. The particle size of dry nanosized copper−zinc alloy powder is below 150 nm as determined by Transmission Electron Microscopy (TEM). Agglomerates of dry nanosized copper−zinc alloy have a primary size of about 70 nm.

4P/16 Metallic zinc powder is available from Umicore. This grade has an average particle size of 3.4−3.9 μm, with a typical average value of 3.6 μm. 4P/32 Metallic zinc powder (Umicore) has an average

Received: December 6, 2010
Accepted: January 17, 2011
Published: February 3, 2011

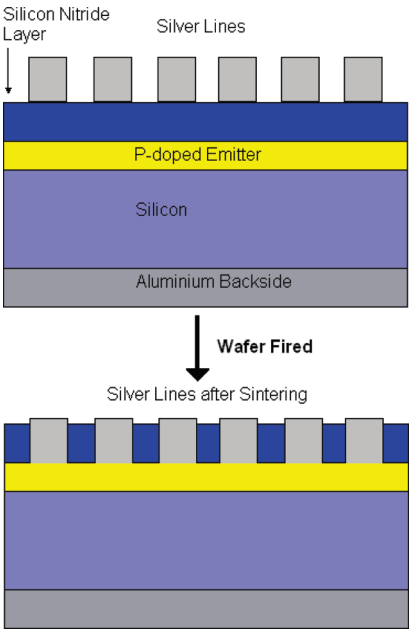

Figure 1. Schematic representation of a silicon cell, showing the metallization paste penetrating the silicon nitride antireflection coating and making contact with the emitter layer after firing.

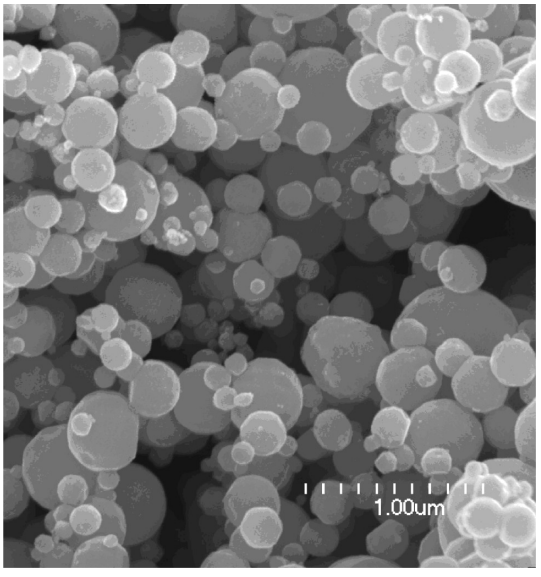

Figure 2. SEM image of metallic nanozinc from Umicore.

particle size of 3.9−4.9 μm, with a typical average value of 4.4 μm. Organic medium consists of an ethyl cellulose resin dispersed in Texanol.

General Paste Preparation. The following procedure was used for paste preparations: The appropriate amounts of solvent, medium and surfactant were mixed in a mixing can for 15 min, then glass frits and nanosized additives were added and mixed for another 15 min. Ag was added incrementally to ensure better wetting. When well-mixed, the paste was repeatedly passed through a 3-roll mill at progressively increasing pressures from 0 to 400 psi. The gap of the rolls was adjusted to 1 mil. The degree of dispersion was measured by fineness of grind (FOG). The FOG values were between 6/4 and 12/6 for our pastes.

The glass frit used in the following examples was milled to a D_{50} of 0.5−0.7 μm prior to use.

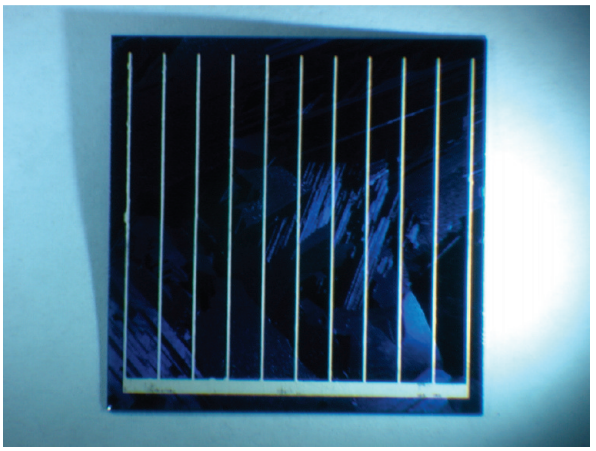

Figure 3. Typical front side of a 1 in. × 1 in. multicrystalline silicon PV cell, printed with 11 silver fingers and one busbar.

Preparation a 50 g Sample of Paste with 5% Nanozinc. Nanozinc (2.5 g) was added to 1 g of glass frit, followed by the addition of 40.5 g of silver. The resulting mixture was then placed on a jar mill to roll for 1 h.

The organics were mixed by adding 0.90 g of the above-discussed organic medium, followed by the addition of 1.00 g of a cohesion additive. Then, 1.25 g of a surfactant was added, followed by 0.25 g of a rheological additive. Finally, 1.75 g of a high boiling oxygenated solvent was added.

The organics were mixed in a Thinky mixer (Thinky USA) for thirty seconds. Thinky is a high speed counter rotational mixer used for mixing and de-airing viscous paste-like materials. Then the inorganic fraction was added to the organic fraction in 3 equal aliquots, with thirty seconds of mixing in the Thinky between each addition. There was 0.85 g of solvent hold-back to adjust the viscosity to the desired level needed for the printing method.

Preparation of a 50 g Sample of Paste with 10% Copper−Zinc Alloy. Copper−zinc alloy nanopowder (5 g) was added to 0.949 g of glass frit. Then, 38.44 g of silver were added, and the resulting mixture was placed on a jar mill to roll for 1 h.

The organics were mixed by adding 0.854 g of the above-discussed organic medium, followed by addition of 0.949 g of a cohesion additive. Then, 1.186 g of a surfactant was added, followed by 0.237 g of a rheological additive and then 1.661 g of a high boiling oxygenated solvent.

The organics were mixed in a Thinky mixer for thirty seconds. Then, the inorganic fraction was added to the organic fraction in 3 equal aliquots, with thirty seconds of mixing in the Thinky between each addition. There was 0.85 g of solvent hold-back to adjust the viscosity to the desired level needed for the printing method.

Screen-Printing Conditions. The pastes were screen-printed on 1 × 1 in.^{2}, 200 μm thick, 65 Ω/□ multicrystalline wafers. The screen-printed pattern was 11 fingers with a busbar, as shown in Figure 3. A screen-printer made by AMI was used in all our experiments.

Commercially available silver paste PV159 (E. I. du Pont de Nemours and Company, Wilmington, DE) was used as a standard. Aluminum paste PV 381 (DuPont) was used to print a backside electrode. The screen for printing the back-side was 230 mesh, 1.4 mil wire, and 0.4 mil emulsion. The screen for printing the Ag front-side was 325 mesh, 0.9 mil wire, 1 mil emulsion, 100 μm line width. The firing program was designed to run at 900, 910, 920, 930, and 945 °C as the peak furnace temperature set points. Five cells were run at each set point.

Test Procedure Efficiency. The solar cells built according to the method described herein were placed in a commercial IV tester for

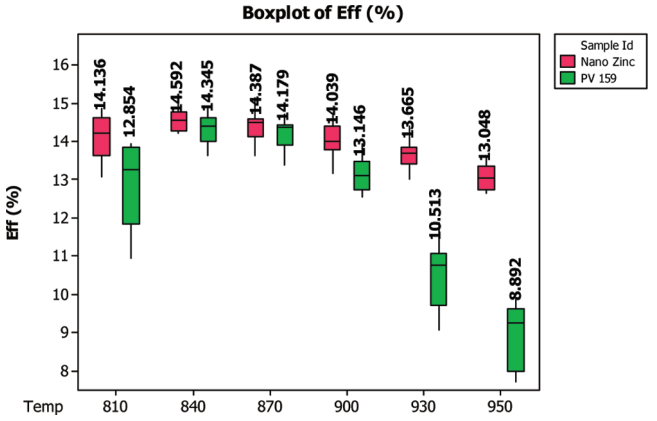

Figure 4. Boxplot of efficiencies of silver paste with 5 wt % nanozinc additive versus PV 159 control. 5 wt % nanozinc loading was determined to be the best for peak efficiency increase.

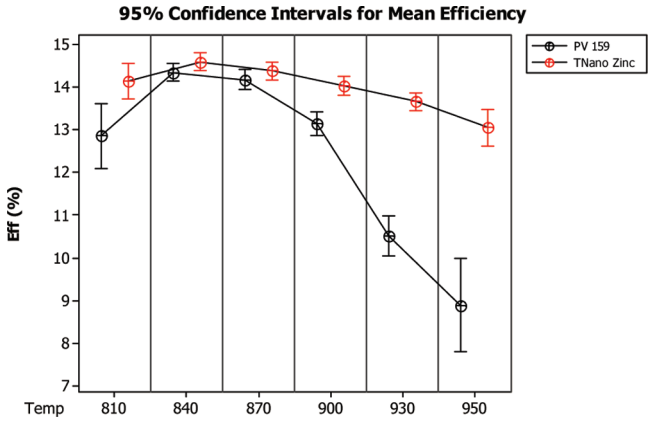

Figure 5. 95% confidence intervals for the mean efficiency of PV 159 and nanozinc silver paste formulations at several firing temperatures.

measuring efficiencies (ST-1000). The Xe Arc lamp in the IV tester simulated sunlight with a known intensity and irradiated the front surface of the cell. The tester used a four-point contact method to measure current (I) and voltage (V) to determine the cell's $I-V$ curve. Fill factor (FF), series resistance (Ra), and efficiency (Eff) were calculated from the $I-V$ curves.

Cell efficiency and fill factor values made using experimental pastes were compared to corresponding values obtained from cells printed with the industry standard silver paste, PV159 (E. I. du Pont de Nemours and Company).

Analytical Methods. Advanced electron microscopy techniques have been used in our study. Dual beam (focused ion and electron) microscopy of FEI's Nanolab has an ion beam and electron beam resolutions of 6 and 2 nm, respectively. The resolution of JEOL2010 transmission electron microscope equipped with energy dispersive spectroscopy is better than 0.18 nm. Two-dimensional characterization of Ag crystallites at the interface was carried out according to the following established method: a HNO_3 soak first dissolved bulk Ag, followed by buffered-HF etching[8] that selectively removed residual interfacial glass. The resulting emitter surface was then imaged with SEM 2-D contact resistance maps of fired cells were also obtained using a SunLab Corescan instrument.[14] The Corescan method is based on the mapping of the potential on the front surface of a solar cell. The method of contact resistance determination is based on the measurement of the potential jump at the boundary between a metal line and the silicon adjacent to it, while a current flows from the silicon into the metal line. The line contact resistance can be calculated by dividing this potential jump by the current flow into the line (per unit length of line). In the Corescan method, light current is locally generated by a small light beam; current flow is enabled by short-circuiting the cell externally. A potential probe centered in the beam measures the local potential and moves together with the beam over the cell, while being continuously in contact with the surface. The probe is always scanned perpendicular to the metal lines. By making parallel scan lines the potential can be determined on the entire cell, and these data are presented within the Corescan software by 2D or 3D graphs.

3. RESULTS AND DISCUSSION

Figure 4 represents the efficiencies of the silver paste prepared with nanozinc additives versus the commercial PV159 standard. Analysis of the data was performed using the Minitab software package. Data means were compared for each of the firing temperatures using 2-sample t tests. The 95% confidence intervals for the mean shown in Figure 5 are a graphical representation of those tests. Results are tabulated in Table 1.

Table 1. Efficiencies of PV 159 and Nano-Zinc Silver Paste Formulations over a Range of the Furnace Hot Zone Set Temperature

		efficiency (%)					
	T (°C)	N	mean	Δ	P (means)	StDev	P (StDevs)
PV 159	810	10	12.854	1.282	0.004	1.069	0.088
nano Zn	810	10	14.136			0.587	
PV 159	840	15	14.345	0.247	0.079	0.362	0.750
nano Zn	840	12	14.592			0.328	
PV 159	870	15	14.179	0.208	0.164	0.418	0.705
nano Zn	870	15	14.387			0.377	
PV 159	900	13	13.146	0.893	0.000	0.452	0.652
nano Zn	900	15	14.039			0.400	
PV 159	930	15	10.513	3.152	0.000	0.870	0.003
nano Zn	930	14	13.665			0.356	
PV 159	950	5	8.892	4.156	0.000	0.883	0.096
nano Zn	950	5	13.048			0.345	

Both formulations reach their peak efficiency at a firing temperature of 840 °C, where the nanozinc mean efficiency is 0.247% higher than that of PV 159. The difference is statistically significant at a confidence level of 90% (P = 0.079). At 870 °C, nanozinc also has a higher mean efficiency, but the difference is not statistically significant (P = 0.164). At all of the other firing temperatures, nanozinc is significantly better than PV 159, with all confidence levels above 99%.

The standard deviations at each temperature were compared using an F test. While the standard deviations are statistically indistinguishable at 840, 870, and 900 °C, the nanozinc formulation is significantly better with at least 90% confidence at 810, 930, and 950. Overall, the nano-Zn efficiency is equal to or better than PV 159 in both mean value and standard deviation across the entire temperature range. The improvements are most dramatic at off-peak temperatures. The improved performance shown in the temperature range 810−870 °C can produce a larger yield of high-efficiency solar cells in a manufacturing facility where cell process variations will occur.

Fill factor follows the same trends as efficiency, as show in Figure 6. The nano-Zn formulation has a higher mean fill factor at all firing temperatures, and the difference is statistically significant

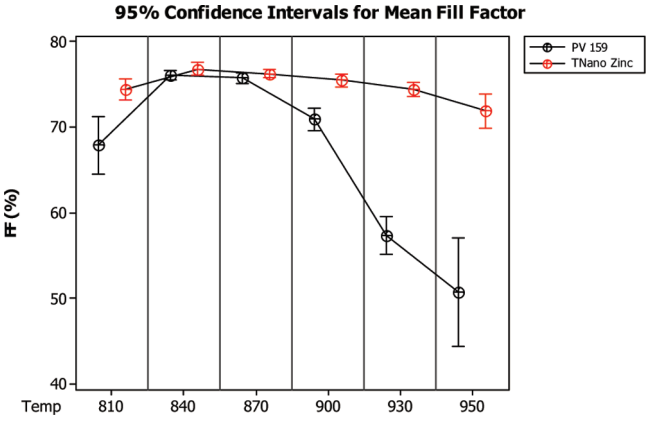

Figure 6. 95% confidence intervals for the mean fill factor of PV 159 and nanozinc silver paste formulations at several firing temperatures.

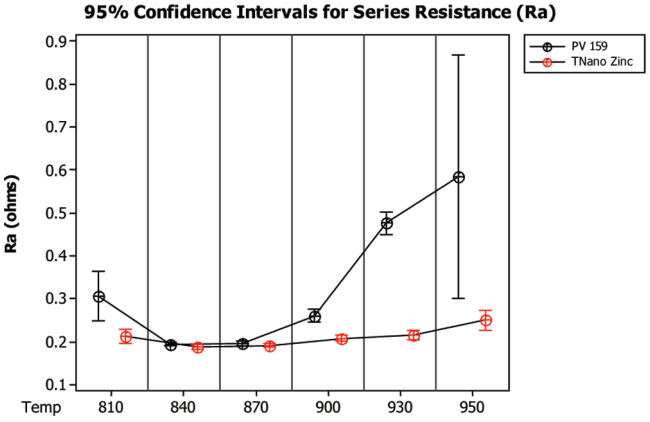

Figure 7. 95% confidence intervals for the mean series resistance (Ra) of PV 159 and nanozinc silver paste formulations at several firing temperatures.

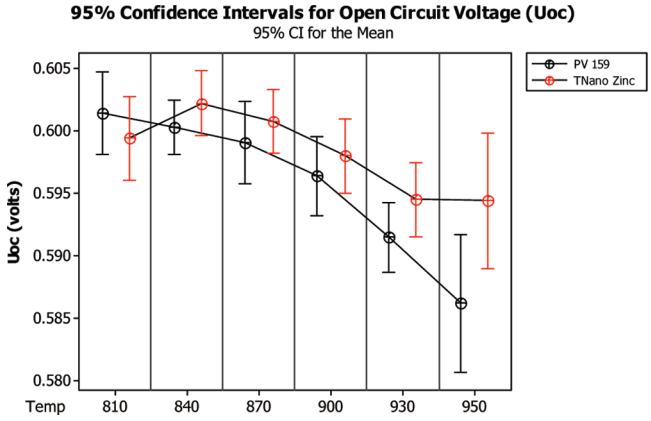

Figure 8. 95% confidence intervals for the open circuit voltage (Uoc) of PV 159 and nanozinc silver paste formulations at several firing temperatures.

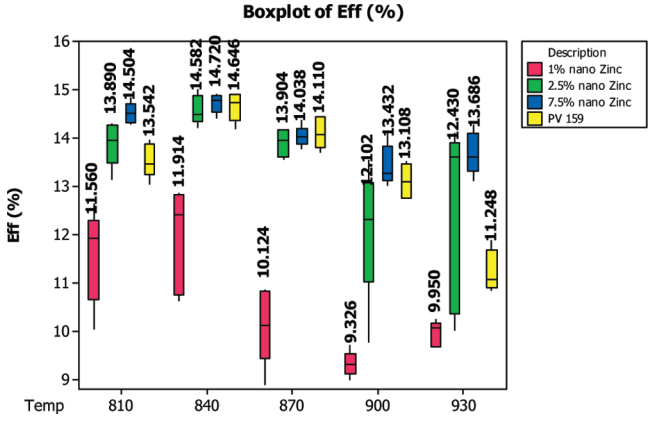

Figure 9. Boxplot of efficiencies versus loadings of nanozinc (1 to 2.5 to 7.5%) in silver pastes. Plot shows the firing window widening with increasing loadings of nanozinc.

with greater than 90% confidence except at 870 °C. Fill factor standard deviations for nano-Zn are statistically indistinguishable from those for PV 159 at 840 and 870 °C, and are lower (with greater than 90% confidence) at the other four firing temperatures.

Series resistance (R_a) is shown in Figure 7. The nanozinc formulation shows a lower and more consistent Ra over the range of firing temperatures. The improvement is statistically significant at greater than 90% confidence for all firing temperatures except 870 °C (see Supporting Information). The standard deviations are lower with greater than 95% confidence at 810, 900, 930, and 950 °C.

Open circuit voltages (U_{oc}), shown in Figure 8, are more similar between the two formulations. There are no statistically significant differences in standard deviations at any firing temperature, and the mean values difference with greater than 95% significance only at a firing temperature of 950 °C (Figure 8).

It is remarkable that even at a loading of nanozinc of only 2.5 wt %, an efficiency of 14.58% was recorded, which is close to the peak of 14.65% for the control paste (Figure 9). Generally, a loading of 2.5−7.5 wt % nanozinc was found to be optimum: 10 wt % nanozinc was detrimental to the electrical properties of the cells, whereas 1% was not sufficient to reach the maximum performance.

In summary, the use of 5% nanozinc as an additive in silver pastes has been shown to result in 0.247% peak efficiency increase at a firing temperature of 840 °C used with the current industry standard paste. Additional beneficial effects include a wider firing window and flatter profiles of the efficiencies and fill factors.

We have also investigated the use of copper−zinc alloy nanopowder as an additive to silver pastes. The efficiencies of PV 159 and a paste made with a copper−zinc alloy are compared in Figure 10. The standard deviations of the two formulations are statistically indistinguishable at all firing temperatures except 870 °C, where the standard deviation of the alloy was unusually high. Both formulations achieve peak efficiency at a firing temperature of 890 °C. The mean efficiencies of the two pastes differ significantly only at the two highest firing temperatures. In both cases, PV 159 has a higher efficiency than the copper−zinc alloy formulations, with better than 99% confidence. Increasing the loading from 10 to 15 wt % copper−zinc alloy nanopowder, did not result in an efficiency gain.

The efficiencies of micrometer-sized zinc particles (3.6 and 4.4 μm) were also compared to nanozinc in the silver paste formulations. 95% confidence levels for each of five firing temperatures are presented in Figure 11. The P values for means reported in the Supporting Information are from an ANOVA analysis, which assumes each subgroup has the same standard

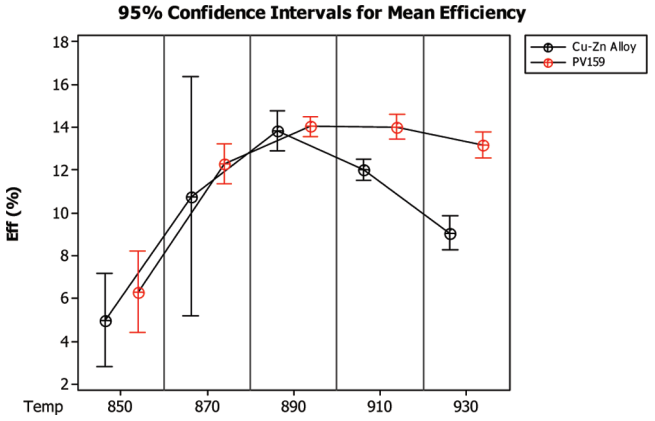

Figure 10. 95% confidence intervals for the mean efficiency of PV 159 and copper−zinc alloy silver paste formulations at several firing temperatures.

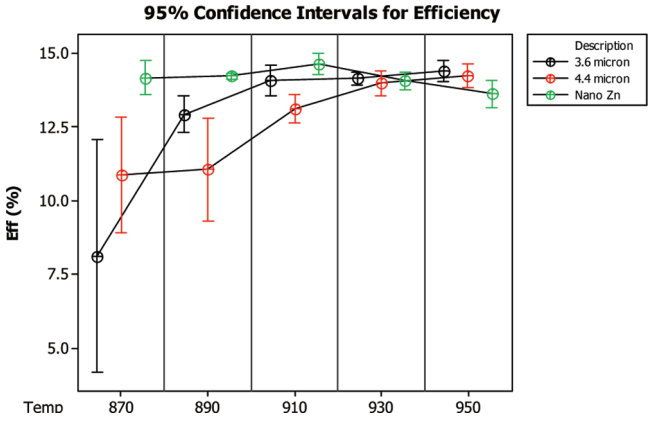

Figure 11. 95% confidence intervals for the mean efficiency of 3.6 μm zinc, 4.4 μm zinc, and nanozinc silver paste formulations at several firing temperatures.

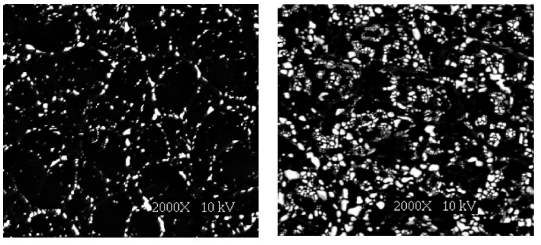

Figure 12. SEM images of Ag crystallites: (a) optimally fired nanozinc cell; (b) overfired nano-Zn cell.

deviation. This is clearly not the case at firing temperatures of 870 and 890 °C, but the ANOVA results are consistent with those from 2-sample *t* tests for each pair of formulations. Those results are tabulated in the Supporting Information.

With greater than 95% confidence, the nanozinc formulation has significantly higher efficiencies than both of the micrometer pastes at firing temperatures of 870, 890, and 910 °C. At 930 °C the three pastes are indistinguishable. At 950 °C, the nanozinc formulation is lower than both of the formulations with micrometer-sized zinc pastes.

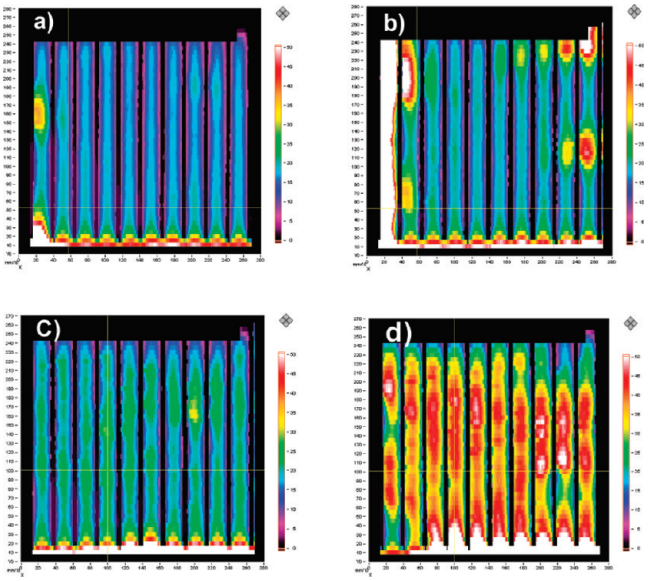

Figure 13. Corescans of silicon cells with metallization pastes prepared with (a) nanozinc and (b) controls at the underfiring temperature of 810 °C and overfiring temperature of 930 °C. The scans show more uniform contact resistance with (c) nanozinc cells than the (d) PV159 cells.

There is a wider firing window of nanozinc pastes vs micrometer-sized zinc pastes. This "flattening" effect is observed on both low and high temperatures extremes. The firing optimum of micrometer-sized pastes is shifted to a higher temperature range. Efficiency distributions for nanozinc are narrower for all temperatures tested vs micrometer-sized alternatives.

To elucidate the possible mechanism of action of nanozinc in silver pastes on silver/silicon nitride/silicon interface, were performed the following analytical experiments, which will be discussed in following section.

Interface Analysis. The aforementioned sequential HNO_3/buffered-HF etching technique was used to expose the surface of the emitter. Numerous SEM top-view images have shown that only a few Ag crystallites were attached to the silicon surface of an optimally fired cell (Figure 12a). In contrast, the overfired cell had more and larger Ag crystallites at the surface of the emitter (Figure 12b). More quantitative image analysis of areal coverage by Ag crystallites readily confirmed the obvious differences between the optimally fired and the overfired cells shown in Figure 12. Currently, there are two plausible mechanisms explaining the current conduction at front-side contact.[1,2] The present study confirms our previous conclusion:[2,15] Ag crystallites are not necessary for current conduction in front-side contact, suggesting "nano-Ag colloid assisted tunneling" plays a dominant role in our nano-Zn cells fired at optimal temperature. However, the size and number of Ag crystallites at the surface of the Si emitter are also an indicator of the degree of silicon nitride etching. We see more Ag crystallites in "nano-Zn" cells than in PV159 cells, suggesting possibly more uniform silicon nitride etching without noticeable emitter damage.

Figure 13 shows Corescans of silicon cells with metallization pastes prepared with nanozinc and PV 159 controls at the underfiring temperature of 810 °C and the overfiring temperature of 930 °C, indicating more uniform contact resistance in the nanozinc cells.

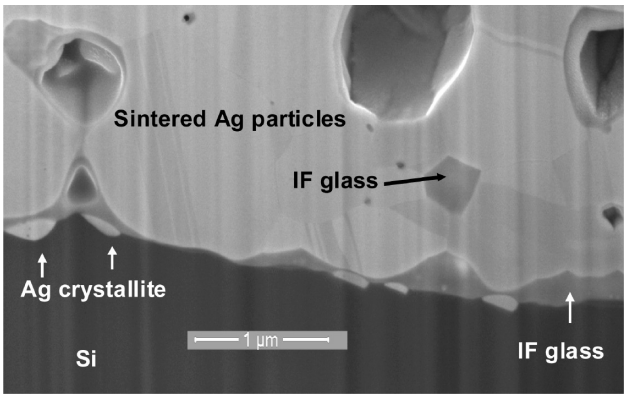

Figure 14. FIB/SEM image of the Ag contact and Si emitter interface in cells printed using a nanozinc-based paste and fired at 950 °C.

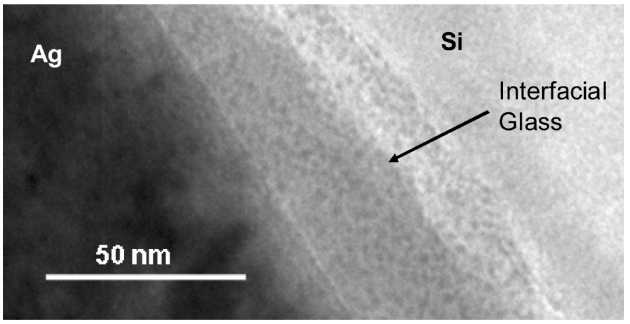

Figure 15. TEM of Ag contact and Si emitter interface.

Figure 14 is a FIB/SEM image shows the complex interfacial microstructure of the Ag contact and Si emitter of a cell printed using a nanozinc paste, and fired at 950 °C. There are Ag crystallites and interfacial glass which contains nano-Ag colloids (for more details, see Figure 15). The remaining silicon nitride insulator layer is much thinner in solar cells printed using nanozinc pastes than those made using PV159 paste. Most of the Ag crystallites at the interface are <1 μm, and do not cause significant shunting (see Sun$-V_{oc}$ results in the Supporting Information). The microstructure of the Ag/Si interface was observed in the commercial pastes similar to PV159 and has already been published.[2,15] The larger Ag crystallites at the Ag/Si interface of the PV159 cell was shown in Figure 12. We believe that the low series resistance seen in Figure 7 may be due to the better silicon nitride etching ability of the nanosized metallic zinc paste.

High-resolution TEM was used to characterize the interface between the front-side contact and the Si emitter. As found by Nakajima,[16,17] the thickness of the interfacial glass between the sintered Ag and Si ranged from a few nanometer to several hundred nanometers. Figure 15 clearly shows that thin interfacial glass of a nanozinc cell fired at optimal condition contains an abundance of nano-Ag colloids, which should dramatically decrease the interfacial resistance and assist in electron tunneling.[18]

4. SUMMARY AND CONCLUSION

Use of nanosized metallic zinc versus micrometer-sized zinc or zinc oxide in silver metallization pastes was found to be beneficial in terms of view of a wider firing window, efficiency, fill factor, and series resistance of multicrystalline silicon cells. It is believed that the dispersed nanozinc provides more uniform etching of the silicon nitride layer resulted in the lower contact resistance at the silver/silicon interface.

■ ASSOCIATED CONTENT

Supporting Information. Statistical analysis of electrical properties and Sun$-V_{oc}$ results (PDF). This material is available free of charge via the Internet at http://pubs.acs.org.

■ AUTHOR INFORMATION

Corresponding Author
*E-mail: alex.s.ionkin@usa.dupont.com.

■ ACKNOWLEDGMENT

The authors thank Marko Strukelj, Steve Freilich and Patrick O'Callaghan for encouragement and guidance. We are grateful to Liang Liang for electron microscopy images, and to Karin Karel for helpful discussion of this study and for proofreading the manuscript.

■ REFERENCES

(1) Ballif, C.; Huljic, D.; Willeke, G.; Hessler-Wyser, A. *Appl. Phys. Lett.* **2003**, *82*, 1878.
(2) Li, Z. G.; Liang, L.; Cheng, L. K. *J. Appl. Phys.* **2009**, *105*, 66102.
(3) Luque, A., Hegedus, S. *Handbook of Photovoltaic Science and Engineering*; John Wiley & Sons: Chichester, U.K., 2003.
(4) Nijs, J. F.; Szlufcik, J.; Poormans, J.; Sivothaman, S.; Mertens, R. P. *IEEE Trans. Electron Devices* **1999**, *46*, 1948.
(5) The information on PV metallization pastes can be found at following Web site: http://www2.dupont.com/Photovoltaics/en_US/products_services/metallization/
(6) Carroll, A. F.; Hang, K. W. U.S. Patent 7 435 362 B2. Issued October 14, 2008.
(7) Hong, K.-K.; Cho, S.-B.; You, J. S.; Jeong, J.-W.; Bea, S.-M.; Huh, J.-Y. *Sol. Energy Mater. Sol. Cells* **2009**, *93* (6 + 7), 898.
(8) Hilali, M.; Nakayashiki, K.; Khadilkar, C.; Reedy, R.; Rohatgi, A.; Shailh, A.; Kim, S.; Sridharan, S. *J. Electrochem. Soc.* **2006**, *153*, A5.
(9) Krebs, F. C. *Sol. Energy Mater. Sol. Cells* **2009**, *93* (4), 484.
(10) Lin, C.; Chung, D. D. L. *J. Mater. Sci.* **2007**, *42*, 9245.
(11) Park, S. H.; Seo, D. S.; Yang, G. S.; Lee, J. K. *Proceedings of the SPIE International Conference on Smart Materials and Nanotechnology in Engineering*; Society of Photo-Optical Instrumentation Engineers: Bellingham, WA, 2007; Vol. 6423, pp 64235J/1−64235J/6
(12) Yue, G.-Z.; Sivec, L.; Owens, J. M.; Yan, B.-J.; Yang, J.; Guha, S. *Appl. Phys. Lett.* **2009**, *95*, 263501.
(13) Further information can be found at the following Umicore Web site: http://www.zincchemicals.umicore.com/zcProducts/fineZincPowders/NanoZincPowderNozip/
(14) (a) Van der Heide., A. S. H., Schonecker, A., Wyers, G. P., Sinke, W. C. *Proceedings of the 16th European Photovoltaic Solar Energy Conference*; Glasgow, U.K., May 1−5, 2000 ; CPL Scientific: Berks, U.K., 2000; pp 1438−1443. (b) www.sunlab.nl/corescan
(15) Cheng, L. K.; Liang, L.; Li, Z. G. *Proceedings of the 34th IEEE Photovoltaic Specialists Conference*; Philadelphia, PA ; IEEE: Piscataway, NJ, 2009.
(16) Nakajima, T.; Kawakami, A.; Tada, A. *Inter. J. Hybrid Microelectronics* **1983**, *6*, 580.
(17) Young, R. J. S.; Carroll, A. F. *Proceedings of the 16th European Photovoltaic Solar Energy Conference*; Glasgow, U.K., May 1−5, 2000 ; CPL Scientific: Berks, U.K., 2000; p 1731.
(18) Roy, B.; Chakravorty, D. *J. Phys.: Condens. Matter* **1990**, *2*, 9323.